GEOPHYSICAL RESEARCH LETTERS, VOL. ???, NO. , PAGES 1–14,

Modeling the effects of radial diffusion and plasmaspheric hiss on outer radiation belt electrons

M. M. Lam,[1] R. B. Horne[1], N. P. Meredith,[1] and S. A. Glauert[1]

Mai Mai Lam, Richard B. Horne, Nigel P. Meredith, and Sarah A. Glauert, British Antarctic Survey, Natural Environment Research Council, High Cross, Madingley Road, Cambridge, CB3 0ET, U.K. (M.Lam@bas.ac.uk)

[1]British Antarctic Survey, Cambridge, UK.

Abstract. We simulate the behaviour of relativistic (976 keV) electrons in the outer radiation belt ($3 \leq L \leq 7$) during the first half of the CRRES mission. We use a 1d radial diffusion model with losses due to pitch-angle scattering by plasmaspheric hiss expressed through the electron lifetime calculated using the PADIE code driven by a global K_p-dependent model of plasmaspheric hiss intensity and f_{pe}/f_{ce}. We use a time and energy-dependent outer boundary derived from observations. The model reproduces flux variations to within an order of magnitude for $L \leq 4$ suggesting hiss is the dominant cause of electron losses in the plasmasphere near the equator. At $L = 5$ the model reproduces significant variations but underestimates the size of the variability. We find that during magnetic storms hiss can cause significant losses for $L \leq 6$ due to its presence in plumes. Wave acceleration is partially represented by the boundary conditions.

1. Introduction

The energetic electron flux ($E > 100$ keV) in the Earth's outer radiation belt ($3 < L < 7$) can vary by up to five orders of magnitude [*Baker and Kanekal*, 2007] on timescales of hours to weeks due to competing acceleration, transport, and loss processes. Understanding and specifying this variability is important because enhanced fluxes of energetic electrons damage satellites [*Wrenn et al.*, 2002] and are a hazard for astronauts.

Transport of relativistic ($\sim$ MeV) electrons within the radiation belts is dominated by radial diffusion. However, quantifying electron loss and acceleration due to resonant interactions with plasma waves is essential for the development of dynamic radiation belt models. Losses due to whistler mode waves, known as plasmaspheric hiss, have been included into transport models [*Beutier and Boscher*, 1995; *Boudarie et al.*, 1997; *Brautigam and Albert*, 2000; *Shprits et al.*, 2005], as well as acceleration and loss due to whistler mode chorus [*Horne et al.*, 2006] with various degrees of success.

Inside the high density plasmasphere previous studies have represented loss due to plasmaspheric hiss by a parameterized loss timescale [*Shprits and Thorne*, 2004; *Shprits et al.*, 2005]. Here, we present a model that incorporates radial transport with energy dependent loss due to plasmaspheric hiss. We use a statistical model based on CRRES data for the observed wave intensity and the ratio of the electron plasma to electron gyro frequency f_{pe}/f_{ce}, as a function of geomagnetic activity (K_p index) with resolution in L shell and magnetic local time (MLT) [*Meredith et al.*, 2004]. As a result, no plasmapause model is required, losses due to hiss within high density plumes are included, and flux variations at 976 keV are reproduced with increasingly good agreement with data as L decreases.

2. Modeling Radial Diffusion with Losses

Theory shows that gradients in electron phase space density f are reduced by radial diffusion across the magnetic field driven by global scale fluctuations in the Earth's mag-

netic and electric fields. Radial diffusion is enhanced when ULF waves are present [e.g., *Elkington et al.*, 1999] at frequencies comparable to the electron drift frequency around the Earth ($\sim$ few mHz at 1 MeV). Since the drift frequency is much lower than the frequencies associated with the bounce ($\sim$ Hz) and gyro ($\sim$ kHz) motion of electrons the first two adiabatic invariants, μ and (Kaufmann) K, are conserved. The first invariant is given by

$$\mu = p^2 sin^2\alpha/(2m_0B) \tag{1}$$

where p is the relativistic electron momentum, m_0 is electron rest mass, B is the magnitude of the Earth's ambient magnetic field and α is the electron's pitch angle. The invariance of μ means that electrons transported towards (away from) the Earth due to radial diffusion are accelerated (decelerated). The evolution of f at constant μ and J is given by [*Schultz and Lanzerotti*, 1974]

$$\frac{\partial f}{\partial t} = L^2 \frac{\partial}{\partial L}\left[D_{LL}L^{-2}\frac{\partial f}{\partial L}\right] - \frac{f}{\tau} \tag{2}$$

where the first term on the right-hand-side is due to radial diffusion (D_{LL} is the radial diffusion coefficient) and the second term is due to losses (where τ is the electron lifetime). Here local acceleration due to gyro-resonant wave particle interactions is not included. A dipole magnetic field is used for all calculations. The radial diffusion coefficient used here is due to electromagnetic fluctuations, which dominate that due to electrostatic fluctuations [*Brautigam and Albert*, 2000], and is given by

$$D_{LL} = D_{LL}^M = 10^{0.506K_p - 9.325}L^{10} \tag{3}$$

for K_p = 1 to 6. Radial diffusion is strongly enhanced for large K_p, corresponding to geomagnetic storm periods, particularly at high values of L. Equation 2 is solved using a fully-implicit numerical method with a conservative differencing scheme and spatial and temporal grid resolutions of $\delta L = 0.1L$ and $\delta t = 0.05135$ days. During the short periods that $K_p > 6$, D_{LL} is calculated for $K_p = 6$. The model was run initially to attain a steady

state for $K_p = 3$ with an inner boundary condition $f(L = 3) = 0$, and outer boundary condition described below.

3. Lifetimes due to Plasmaspheric Hiss

The electron loss timescale due to plasmaspheric hiss can be derived from the bounce averaged pitch angle diffusion rate $\langle D_{\alpha\alpha}\rangle/p^2$ averaged over the drift orbit of the electrons around the Earth. Pitch angle diffusion rates depend on several factors, including the wave power, magnetic field strength (and hence L), f_{pe}/f_{ce}, and the frequency and propagation direction of the waves. The loss timescale for ~ 1 MeV electrons due to plasmaspheric hiss is of the order of a few days [*Meredith et al.*, 2006, 2007], much longer than the timescale for electron drift around the Earth, which is about 15 minutes. Since wave power, f_{pe}/f_{ce} and other plasma conditions vary considerably in magnetic local time (MLT), and with magnetic activity, these variations must be taken into account. We use two statistical models comprising data from the CRRES plasma wave experiment [*Anderson et al.*, 1992], one for the wave intensity B_W^2 and the other for f_{pe}/f_{ce}, for three different levels of magnetic activity as measured by K_p (similar to *Meredith et al.* [2004] but binned in K_p rather than AE).

The wave intensity of plasmaspheric hiss, and f_{pe}/f_{ce}, were determined from CRRES data and sorted into a database with a resolution of $0.1L$, and 1 hour MLT for $K_p < 2$, $2 \leq K_p < 4$, and $K_p \geq 4$. Since whistler-mode chorus and fast magnetosonic waves can also occur in the hiss frequency range $0.1 - 5$ kHz they were excluded from the data [*Meredith et al.*, 2004, 2007]. Figure 1a shows plasmaspheric hiss wave intensity as a function of L for the three K_p categories. Wave intensity has been averaged over $5^\circ \leq \lambda_m \leq 30^\circ$ and 24 hours of MLT. Hiss intensity increases with K_p, particularly for $L > 4$, even though the high density plasmapause is known to be eroded to lower L, during high geomagnetic activity. At large L the increase in intensity is mainly restricted to the noon-afternoon MLT sector, resulting in the MLT-mean hiss intensity at $L = 6$

being higher for $2 \leq K_p < 4$ than for $K_p \geq 4$. We attribute the increase to the occurrence of hiss inside high density plumes [e.g. *Meredith et al.*, 2004] which can extend to large L on the dayside during geomagnetic storms and substorms [*Moldwin et al.*, 2004; *Goldstein et al.*, 2004]. Thus hiss at large L, which may be important for electron loss to the atmosphere, is included in our model.

Pitch angle diffusion rates depend on the distribution of wave power in frequency and wave normal angle and were computed using the PADIE code (Pitch Angle and energy Diffusion of Ions and Electrons) [*Glauert and Horne*, 2005]. PADIE assumes a Gaussian distribution in wave power and $X = \tan\psi$ where ψ is the wave normal angle. Following *Meredith et al.* [2006], typical properties for plasmaspheric hiss were used including a peak intensity at 550 Hz, a bandwidth of 300 Hz, and lower and upper cut-off frequencies of 0.1 and 2 kHz. Comparison between observed and model loss timescales during quiet times suggest that electron loss is caused by hiss propagating at small to intermediate wave normal angles ($0^\circ \leq \psi \leq 50^\circ$), and that the sensitivity to wave normal angle in this range is low [*Meredith et al.*, 2004, 2006]. Therefore a Gaussian distribution in X peaked along the magnetic field direction with an angular spread of $X_w = \tan 20^\circ$ was used. Landau and ± 10 cyclotron harmonic resonances were included in the calculations. Interactions between waves and electrons at higher latitudes were taken into account by bounce averaging the diffusion rates between the mirror points, assuming the wave power remains constant and using a constant plasma density and dipole magnetic field. A nominal wave intensity of 900 pT^2 was used, subsequently scaled according to observations in the wave database.

Since pitch angle diffusion rates depend on f_{pe}/f_{ce} [*Horne et al.*, 2003] PADIE was used to calculate a matrix of diffusion coefficients as a function of pitch angle at $L = 3, 4, 5$, and 6, at $f_{pe}/f_{ce} = 2, 6, 10, 14$, and 18, and energies of 10, 20, 50, 100, 200, 500, 1000, 2000, and 5000 keV which encompass observations. As electrons drift around the Earth they encounter different wave and plasma conditions which change the rate of diffusion. We take

account of this global variability in our model. For a given K_p our statistical wave models specify the spatial distribution of wave intensity and f_{pe}/f_{ce}. The bounce-averaged pitch angle diffusion rates were interpolated from the diffusion matrix to the value of f_{pe}/f_{ce}, L and electron energy, scaled by the wave power in each MLT bin, and averaged over 24 hours to obtain the bounce and drift averaged diffusion rates. The precipitation lifetime τ was then obtained by numerically solving the 1d pitch-angle diffusion equation, assuming that the electron distribution function can be separated into a pitch-angle dependent function and a time-dependent function $F(t)$, given by [*Lyons et al*, 1972, *Albert*, 1994]

$$\tau = \frac{-F}{dF/dt} \tag{4}$$

This was done between $L = 3$ and 6 at a resolution of $0.5L$, at the three levels of Kp and the 9 energy levels and kept in a lookup table for use in the model. Electron lifetimes are shown in Figure 1b for a constant energy of $E = 976$ keV. At $L < 3.5$, electron lifetimes only show a small reduction with increasing K_p from about 2.5 days to 1 day. However, for $3.5 < L < 6$ electron lifetimes are more dramatically reduced with increasing magnetic activity, indicating the importance of hiss inside high density plumes.

At $L = 6$ the global electron lifetime is less for $2 \leq K_p < 4$ than for $K_p \geq 4$. This is due to two factors: firstly f_{pe}/f_{ce} at $L = 6$ tends to be higher for high geomagnetic activity than for moderate activity [*Meredith et al.*, 2004] and electron lifetimes calculated by PADIE increase with increasing f_{pe}/f_{ce}. Secondly, hiss intensity is greater at moderate activity than at high magnetic activity (Figure 1a).

4. Outer Boundary Conditions

Since the $\sim$ 1 MeV electron flux at geostationary orbit can vary by several orders of magnitude, a time-dependent outer boundary is used for the radial diffusion model with losses. Equation (2) is solved for multiple values of μ to obtain results at 976 keV for

$3 \leq L \leq 7$ with a resolution of $0.1L$, so the model requires the flux at different energies at the outer boundary at $L = 7$.

Combined Release and Radiation Effects Satellite (CRRES) Medium Electrons A (MEA) observations [*Vampola et al.*, 1992] show that the electron flux often decreases during the main phase of a storm at ~ 1 MeV (e.g., Figure 2b, red line) whereas at 153 keV (blue line) there may be no significant decrease, or even an increase during the storm main phase (e.g. storms 1-4 in Figure 2a). Thus simply scaling the electron flux at one energy to all energies for the outer boundary condition is not sufficient.

Brautigam and Albert [2000] found that coverage of phase space density in μ and K is very limited in the CRRES data set at $L^* > 6$. For their outer boundary condition they developed a method of using geosynchronous data. We use a similar method. Since CRRES MEA data at $L = 7$ has poor time resolution due to orbit constraints, we use data from $L = 6$ which has a much better time resolution (~ 5 hours) and apply this to the outer boundary at $L = 7$ as described below. The variability of the electron flux at each of the 17 MEA energy channels (153-1582 keV) at $L = 6$ was calculated by the ratio

$$R(E,t) = \frac{J(E,t)}{J_q(L=6)} \tag{5}$$

where $J(E,t)$ is the measured flux at $L = 6$ and $J_q(L = 6)$ is the average flux at $L = 6$ measured on quiet day 281, 1990. The flux at the outer boundary ($L = 7$) was then found by multiplying R by the average quiet-time electron energy spectrum at $L = 7$, $J_q(L = 7)$, as done by Shprits and Thorne [2004]. In their paper $J_q(L = 7) = 8222.6 \exp(-7.068W)$ (cm^{-2} s^{-1} sr^{-1} keV^{-1}) where W is the electron energy in MeV. The temporal variation at a required energy was found by interpolation. Although variations faster than a few hours are not captured in the model (Figure 2b), long duration magnetic storms should be reproduced.

5. Electron flux variability

The models for wave intensity and f_{pe}/f_{ce} are for the range $5^\circ \leq \lambda_m \leq 30^\circ$ MLT. In addition, the radial diffusion coefficients were determined for the equator. To test our model against observations we therefore simulate the 90° pitch angle electron flux measured by the CRRES MEA experiment (Figure 3). A time sequence of K_p (Figure 3g) was used to drive the model for a period of $\sim$ 150 days starting from 30 July 1990, corresponding to day of year (DOY) 211.

At $L = 3.5$, the observed electron flux increases by up to three orders of magnitude when geomagnetic activity is high (Figure 3e, green), for instance, at the onsets of storms 1, 3 and 4. Exponential decay follows such increases during quieter periods (e.g. DOY 235-258, DOY 285-330, DOY 332-350). The model decay rate at $L = 3.5$ is in remarkably good agreement with observations showing that the observed quiet-time exponential decays are due to pitch-angle scattering caused by the interaction of the electrons with plasmaspheric hiss. After the onsets of storms 3 and 4, the model flux at $L = 3.5$ starts to decrease when the measured flux is still increasing, contributing to the order of magnitude difference between model and observations. Possible causes for the difference between model results and data include an insufficient resolution in K_p in the statistical wave model, insufficient resolution in time or energy in the data used to derive the outer boundary condition, and the lack of local acceleration processes in the model.

At $L = 5$ (Figure 3c), the model flux tends to increase and decrease at times when there are significant variations in the observed flux, but underestimates the size of the variability. There is also a lot of variability in the data which is not reproduced in the model, although the peak to peak variability in the data is smaller than at $L = 3.5$. This may seem surprising since $L = 5$ is closer to the outer boundary. However, the model reflects variability in the outer boundary. If variations in the outer boundary are relatively small, and last for periods short compared with the time for diffusion from $L = 7$ to $L = 5$ then the flux at $L = 5$ will be smoother than that at $L = 7$. Therefore at least some

of the observed variability at $L = 5$ is probably due to another local process as opposed to inward radial diffusion. $L = 5$ also lies mostly outside the plasmasphere during more disturbed times (the dotted line in Figures 3a and b is an idealized plasmapause from *Carpenter and Anderson* [1992]) and hiss losses are smaller than at lower L.

In a similar study *Shprits et al.* [2005] used a constant outer boundary, and an empirical electron lifetime of $3/K_p$ outside the plasmapause and 10 days within the plasmapause. Their simple parameterization, however, is only applicable at 1 MeV. Our lifetimes are based on more careful analysis of the data and are well below 10 days when $K_p \geq 2$ and even for $K_p < 2$ when $L \leq 4$ (Figure 1b). While *Shprits et al.* [2005] reproduce the variability outside the plasmapause, our model should provide a better representation inside the plasmapause.

6. Concluding remarks

Our model does remarkably well at reproducing flux decay rates at $L = 3.5$ and 4 and simulates the flux to within an order of magnitude. This raises the question of the importance of electron acceleration due to wave-particle interactions, for instance, from whistler mode chorus. *Chen et al.* [2007] found frequent and persistent peaks in phase space density around $L^* = 5.5$ which they suggest is compelling evidence for gyro-resonant wave acceleration. The boundary condition for our model is derived from CRRES MEA data at $L = 6$ which is at a similar location. Thus some of the variability due to local wave acceleration processes is included in the model via the boundary conditions, which may explain why the model performs so well. However, acceleration and losses due to other wave modes are also likely to be important, and more complex models are required to fully understand their role in radiation belt dynamics.

During magnetic storms the plasmasphere becomes eroded and asymmetric in MLT. High density plumes develop and extend towards the magnetopause mainly in the post noon MLT sector. Plumes can contain intense plasmaspheric hiss emissions [e.g., *Summers*

et al., 2007]. Our model includes the effects of hiss in plumes without the need to define a complicated plasmapause structure in MLT. The results show that even though plumes may be confined in MLT, losses due to hiss within plumes can have a significant effect on the electron lifetimes even out to $L = 6$ during magnetically active conditions, and must be included in any physics-based model.

The results show that it is possible to model variations in the outer radiation belt using physics-based models provided time and energy-dependent outer boundary conditions are used. While satellites such as GOES at geosynchronous orbit measure the relativistic electron flux, additional observations at lower energies ($\sim$ 50 keV) are required to model the radiation environment for GPS, Galileo, and lower satellite orbits.

Acknowledgments. We thank Al Vampola and Daniel Heynderickx for providing CRRES MEA data, NSSDC Omniweb for providing the geomagnetic indices and Roger Anderson for providing plasma wave data.

References

Albert, J. M. (1994), Quasi-linear pitch-angle diffusion coefficients: retaining higher harmonics, *J. Geophys. Res.*, *99*(A12), 23741.

Anderson, R. R., D. A. Gurnett, and D. L. Odem (1992), CRRES plasma wave experiment, *J. Spacecr. Rockets*, *29*(4), 570-573.

Baker D. N., and S. G. Kanekal (2007), Solar cycle changes, geomagnetic variations, and energetic particle properties in the inner magnetosphere, *J. of Atmos. and Solar Terr. Phys.*, in press.

Beutier, T., and D. Boscher (1995), A three-dimensional analysis of the electron radiation belt by the *Salammbô* code, *J. Geophys. Res., 100*(A8), 14,853.

Bourdarie, S., D. Boscher, T. Beutier, J. A. Sauvaud, and M. Blanc (1997), Electron and proton radiation belt simulations during storm periods: A new asymmetric convection-diffusion model, *J. Geophys. Res., 102*, 17,541-17,552.

Brautigam, D. H., and J. M. Albert (2000), Radial diffusion analysis of outer radiation belt electrons during the October 9, 1990, magnetic storm, *J. Geophys. Res.*, *105*(A1), 291-309.

Carpenter, D. L., and R. R. Anderson (1992), An ISEE/whistler model of equatorial electron density in the magnetosphere, *J. Geophys. Res.*, *97*(A2), 1097-1108.

Chen, Y., G. D. Reeves, and R. H. W. Friedel (2007), The energization of relativistic electrons in the outer Van Allen belt, *Nature Physics* (01 July 2007) Letters, doi:10.1038/nphys655.

Elkington, S. R., M. K. Hudson, and A. A. Chan (1999), Acceleration of relativistic electrons via drift-resonant interaction with toroidal-mode Pc-5 ULF oscillations, *Geophys. Res. Lett.*, *26*(21), 3273-3276.

Glauert, S. A., and R. B. Horne (2005), Calculation of pitch angle and energy diffusion coefficients with the *PADIE* code, *J. Geophys. Res.*, *110*, A04206, doi: 10.1029/2004JA010851.

Goldstein, J., B. R. Sandel, M. F. Thomsen, M. Spasojevíc, and P. H. Reiff (2004), Simultaneous remote sensing and in situ observations of plasmaspheric drainage plumes, *J. Geophys. Res., 109*, A03202, doi:10.1029/2003JA010281.

Horne, R. B., S. A. Glauert, and R. M. Thorne (2003), Resonant diffusion of radiation belt electrons by whistler-mode chorus, *Geophys. Res. Lett.*, *30*(9), 1493, doi:10.1029/2003GL016963.

Horne, R. B., N. P. Meredith, S. A. Glauert, A. Varotsou, D. Bosher, R. M. Thorne, Y. Y. Shprits, and R. R. Anderson (2006), Mechanisms for the acceleration of radiation belt electrons, in *Recurrent Magnetic Storms: Corotating Solar Wind Streams, Geophys. Monogr. Ser.*, vol. 167, edited by B. T. Tsurutani, R. L. McPherron, W. D. Gonzalez, G. Lu, J. H. A. Sobral, and N. Gopalswamy, pp. 151-173, AGU, Washington, D.C.

Lyons, L. R., R. M. Thorne, and C. F. Kennel (1972), Pitch-angle diffusion of radiation belt electrons within the plasmasphere, *J. Geophys. Res.*, *77*(19), 3455-3474.

Meredith, N. P., R. B. Horne, R. M. Thorne, D. Summers, and R. R. Anderson (2004), Substorm dependence of plasmaspheric hiss, *J. Geophys. Res.*, *109*, A06209, doi:10.1029/2004JA010387.

Meredith, N. P., R. B. Horne, S. A. Glauert, R. M. Thorne, D. Summers, J. M. Albert, and R. R. Anderson (2006), Energetic outer zone electron loss timescales during low geomagnetic activity, *J. Geophys. Res., 111*, A05212, doi:10.1029/2005JA011516.

Meredith, N. P., R. B. Horne, S. A. Glauert, and R. R. Anderson (2007), Slot region electron loss timescales due to plasmaspheric hiss and lightning-generated whistlers, *J. Geophys. Res., 112*, A08214, doi:10.1029/2007JA012413.

Moldwin, M. B., J. Howard, J. Sanny, J. D. Bocchicchio, H. K. Rassoul, R. R. Anderson (2004), Plasmaspheric plumes: CRRES observations of enhanced density beyond the plasmapause, *J. Geophys. Res.*, *109*, A05202, doi:10.1029/2003JA010320.

Schulz, M., and L. J. Lanzerotti (1974), *Particle diffusion in the radiation belts*, Springer-Verlag, New York.

Shprits, Y. Y., and R. M. Thorne (2004), Time dependent radial diffusion modeling of relativistic electrons with realistic loss rates, *Geophys. Res. Lett., 31*, doi:10.1029/2004GL019591.

Shprits, Y. Y., R. M. Thorne, G. D. Reeves, and R. Friedel (2005), Radial diffusion modeling with emprical lifetimes: comparison with CRRES observations, *Ann. Geophys.*, *23*, 1467-1471.

Summers, D. B. Ni, N. P. Meredith, R. B. Horne, R. M. Thorne, M. B. Moldwin, and R. R. Anderson (2007), Electron scattering by whistler-mode ELF hiss in plasmaspheric plumes, *J. Geophys. Res.,* submitted.

Vampola, A. L., J. V. Osborn, and B. M. Johnson (1992), CRRES magnetic electron spectrometer, *J. Spacecr. Rockets*, *29*(4), 592.

Wrenn, G. L., D. J. Rodgers, and K. A. Ryden (2002), A solar cycle of spacecraft anomalies due to internal charging, *Ann. Geophys*, *20*(7), 953-956.

Figure 1. (a) The average over MLT of the plasmaspheric hiss wave intensity B_W^2 in the wave model, and (b) the global electron lifetime τ for E=976 keV.

Figure 2. The electron differential flux at $L = 6$ for a pitch angle of 90° from CRRES MEA data, at an energy of 976 keV (red) and 153 keV (purple). (a) The dotted vertical lines mark the onset times of the large geomagnetic storms whose onsets occur at: (1) DOY 233, (2) DOY 238, (3) DOY 282, and (4) DOY 330. (b) The CRRES MEA data (diamonds) and the data interpolated onto the 1d radial diffusion model time grid (solid) around onset of storm 3.

Figure 3. A comparison of CRRES MEA data with the 1d radial diffusion model for an electron energy of 976 keV and pitch angle of 90°: (a) CRRES MEA electron flux (bad data points in gray); (b) model. Electron flux from: CRRES MEA data (green) and the model (blue) at (c) L=5, (d) L=4, and (e) L=3.5. The vertical dotted lines mark the onset times of four large geomagnetic storms. The geomagnetic indices (f) D_{st} and (g) K_p.

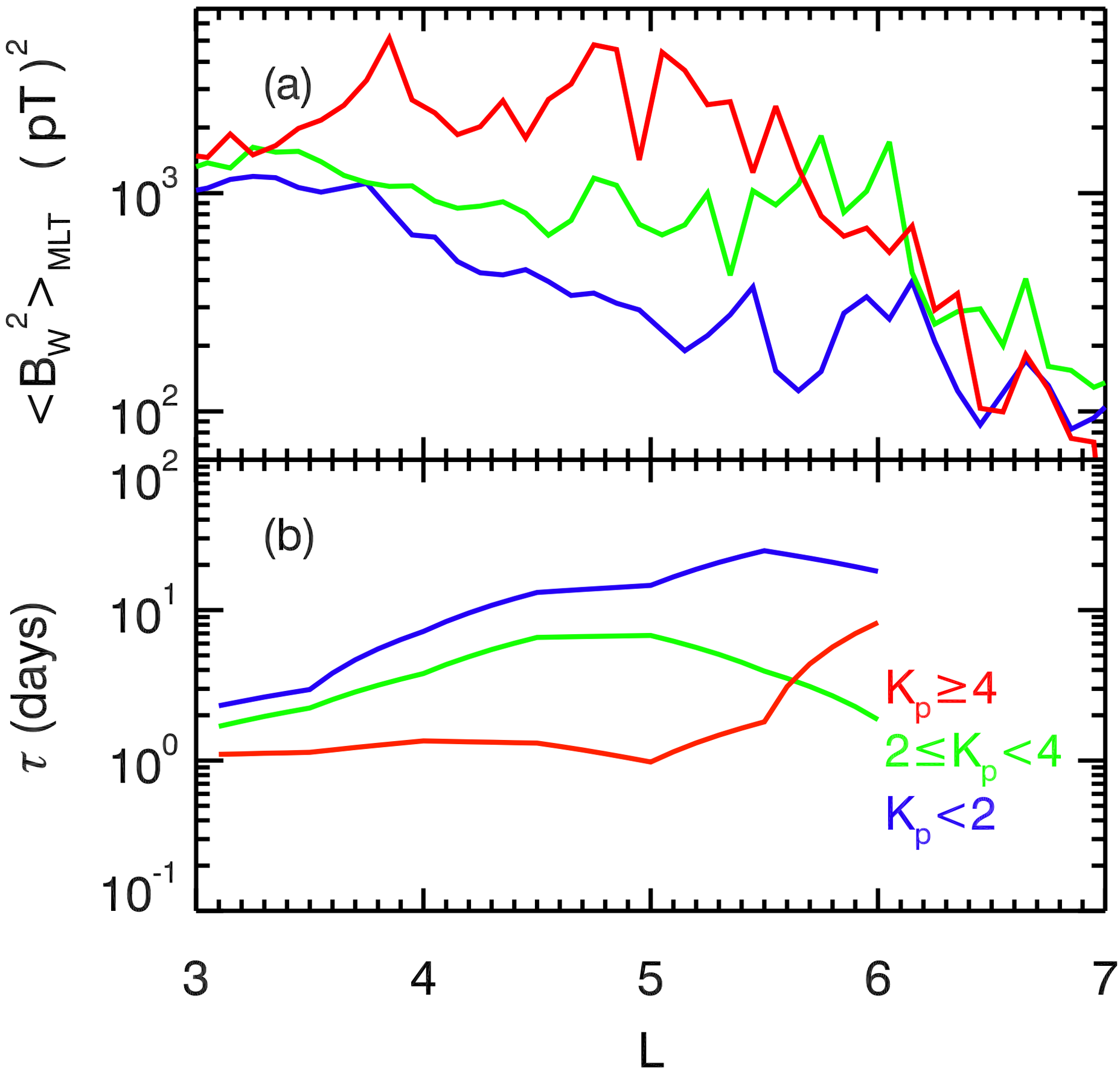
(a)
(b)
$<B_W^2>_{MLT}$ (pT)^2
τ (days)
10^3
10^2
10^2
10^1
10^0
10^{-1}
$K_p \geq 4$
$2 \leq K_p < 4$
$K_p < 2$
3
4
5
6
7
L

Figure 1

Figure 2

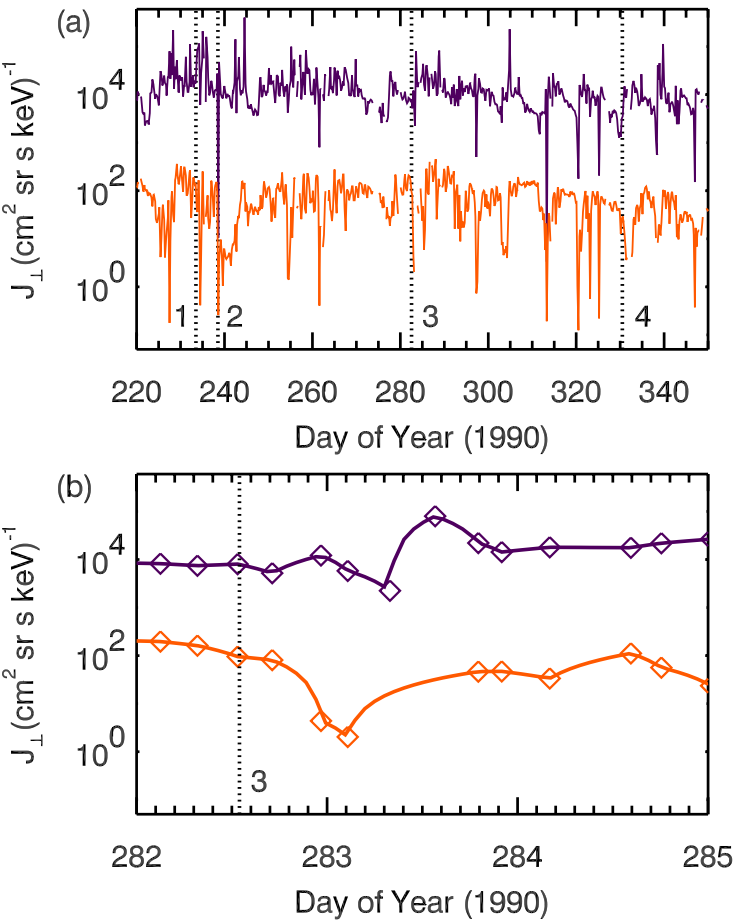
(a)
$J_\perp$ (cm^2 sr s keV)$^{-1}$
10^4
10^2
10^0
1
2
3
4
220
240
260
280
300
320
340
Day of Year (1990)
(b)
$J_\perp$ (cm^2 sr s keV)$^{-1}$
10^4
10^2
10^0
3
282
283
284
285
Day of Year (1990)

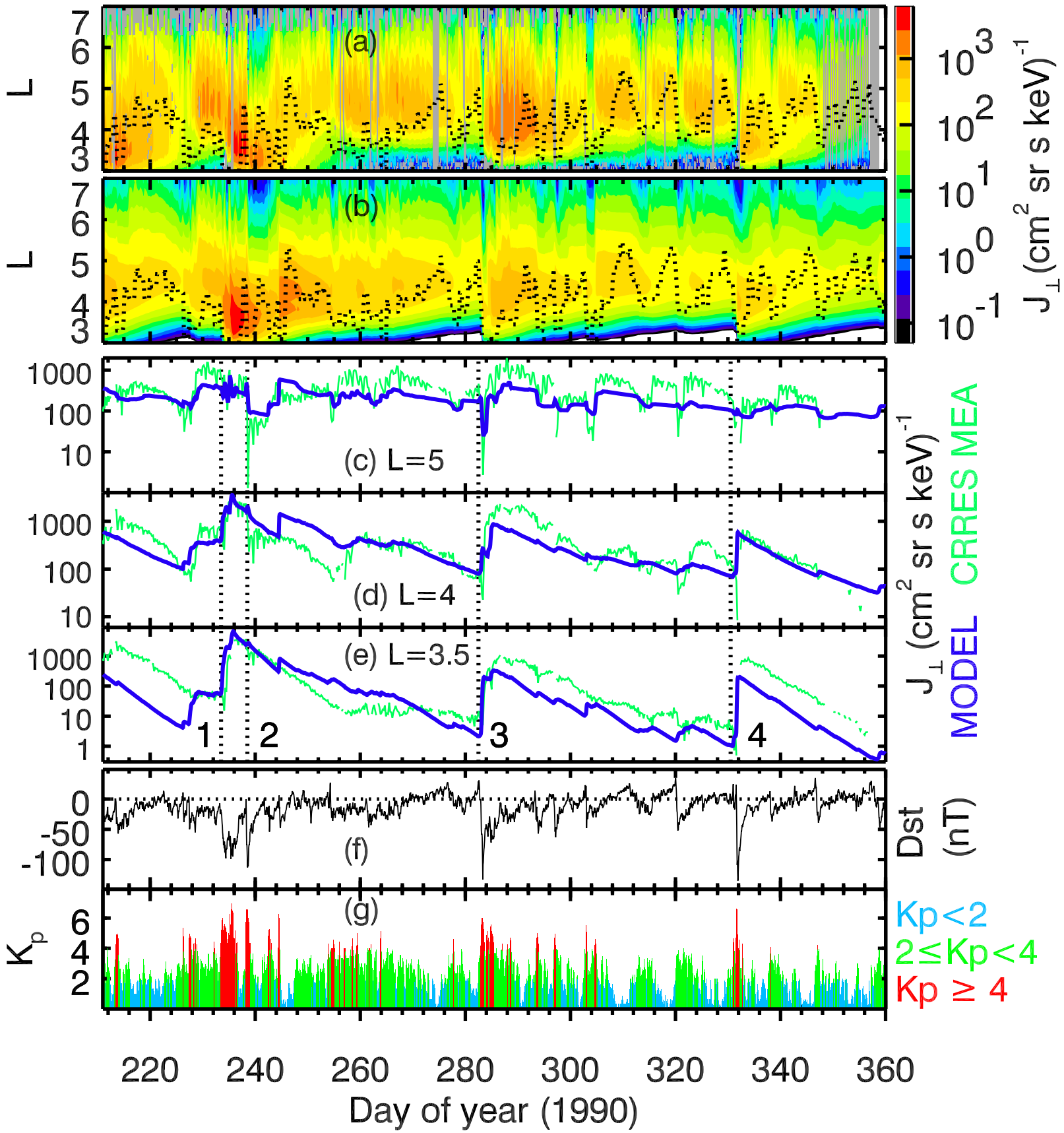
(a)
(b)
L
7
6
5
4
3
10^3
10^2
10^1
10^0
10^{-1}
$J_\perp$ (cm^2 sr s keV)$^{-1}$
1000
100
10
1
(c) L=5
(d) L=4
(e) L=3.5
1
2
3
4
MODEL
CRRES MEA
0
-50
-100
(f)
Dst (nT)
K_p
(g)
Kp<2
2≤Kp<4
Kp ≥ 4
220
240
260
280
300
320
340
360
Day of year (1990)

Figure 3